Definition, classification and morphometry of entrance of the bicipital groove and its associations with lesions of adjacent structures

Shiguo Yuan
Southern Medical University https://orcid.org/0000-0003-3781-6786
Yucong Zou
Southern Medical University
Kai Zheng
Youjiang Medical University for Nationalities
Xuecheng Huang
Southern Medical University
Zhiwei Zhang
Hainan Province Hospital of Traditional Chinese Medicine
Yanping Gao
Southern Medical University
Yikai Li
Southern Medical University
Xiaochun Bai (baixc15@smu.edu.cn)
The Third Affiliated Hospital of Southern Medical University

Research article

Keywords: Shoulder pain, bicipital groove, biceps pulley complex, biceps brachii tendon, anatomy, images, classification

Posted Date: August 26th, 2020

DOI: https://doi.org/10.21203/rs.3.rs-57253/v1

Abstract

Background

The definition of the entrance of the bicipital groove (EBG) is still unclear, and the relationships between the EBG and lesions of the long head of the biceps brachii tendon (LBT) and biceps pulley complex (BPC) have long been controversial. The purpose of this anatomic and imaging study was to define the EBG and to examine morphological parameters, classifications, and their relationships with lesions of the LBT and BPC.

Methods

One hundred thirteen unpaired intact dry humeri, 34 cadaveric shoulder specimens and 278 shoulder images were collected, measured, and classified based on morphological characteristics. Soft tissue and bony landmarks of the EBG were classified into different types. The relationships between the types and lesions of the LBT and BPC were analyzed through an anatomic and imaging study.

Results

Type *II*, type *A* and type *i* of the EBG and type *b* of the adjacent articular surface accounted for most of the dry humeri, cadavers, and images. Based on the EBG classification in the superoinferior image view, all of the subluxations and dislocations were classified as type *B* (61/120, 50.83%; $\chi2 = 16.55$, $P < 0.001$), and most LBT and BPC lesions were type *B* (65/117, 55.56%; $\chi2 = 26.05$, $P < 0.001$). LBTs were injured in ($\chi2=$, $P < 0.001$) 83.56% of type *B*, 100% of type *C*, and 95.83% of type *iii* EBGs ($\chi2 = 135.69, 31.89$, all $P < 0.001$). Similarly, BPCs were injured in 89.04% of type *B* and 93.10% of type *C* EBGs ($\chi2 = 153.14$, $P < 0.001$), while BPCs were injured in 95.8% of type *iii* EBGs ($\chi2 = 33.79$, $P < 0.001$).

Conclusions

The EBG is an anatomical concept worthy of clinical attention. Anatomical variations in the EBG correlated with lesions of the LBT and BPC. LBT and BPC lesions correlated with type *B* and *C* EBGs by imaging analysis.

Introduction

Shoulder pain is one of the most common musculoskeletal complaints, and many diseases, including tendinitis and tenosynovitis of the long head of the biceps brachii tendon (LBT), rotator cuff disease and lesions of the biceps pulley complex (BPC), are origins of shoulder pain[1, 2]. These origins usually involve a key anatomical structure—the entrance of the bicipital groove (EBG)[3]. The bicipital groove lies between the greater and lesser tuberosity of the humerus through which the LBT passes[4]. The

transverse humeral ligament passing from the lesser tuberosity to the greater tuberosity of the humerus overlies the LBT as it emerges from the capsule of the shoulder joint[5]. The subscapularis tendon, coracohumeral ligament, and transverse humeral ligament are all believed to contribute to LBT stability within the bicipital groove[6]. Although many studies have examined the pathology of EBG-related lesions, the definition of the EBG remains equivocal.

The relationship between variations in the anatomical structure of the EBG and local lesions or injury is controversial. Several articles have reported that the morphology of the bicipital groove affects LBT disorders[7–9]; some anecdotal studies have not supported any correlation between intra-articular biceps tendon pathology and bicipital groove morphology[10]. Some authors have argued that the transverse ligament does not exist as a separate entity[5, 11] but is considered as an extension of the subscapularis tendon and only contributes slightly to the stabilization of the LBT in the bicipital groove[12].

In order to clarify the dispute, we developed a clear definition of the EBG as an anatomic and functional segment along the LBT from the upper margin of the transverse humeral ligament to the intra-articular soft tissue (synovium, a hammock-like synovial sling or part of the BPC) surrounding the LBT adjacent to the entrance of the capsule (Fig. 1A). The EBG is a channel with variable length and a constant position and consists of two parts: an intra-articular segment and an extra-articular segment. The intra-articular segment of the EBG is a soft tissue channel wrapping the LBT near entrance of the capsule. The extra-articular segment is a semiosseous channel from the entrance of the capsule to the upper margin of the transverse humeral ligament. Usually, the level of the upper margin of the transverse humeral ligament is the turning point for a cliff of the lesser tuberosity (Fig. 1A, 1B). Additionally, we classified anatomical landmarks of the EBG to examine their correlations with lesions of the LBT and BPC in an anatomic and imaging study.

Materials And Methods

The research was reviewed by the Medical Ethics Committee of Hainan Province Hospital of Traditional Chinese Medicine (approval number: 2020015) and Human Research Ethics Committee of the Third Affiliated Hospital of Southern Medical University (approval number: 2020-015-003).

Cadaveric specimens

Cadaveric shoulders were supplied by the Department of Anatomy, School of Basic Medicine, Southern Medical University, China. Measurements and observations were performed on 34 unpaired adult shoulders from cadaveric specimens without visible evidence of pathologic processes (tumor, infection, or fracture). The BPC was checked for lesions after removing the deltoid muscle, and then the capsule was incised to assess the EBG, LBT and BPC.

The length, width, depth, and angles of the EBG were measured[9, 13-15] (Figure 1B and Figure 6A, 6B, 6C). Lesions of the LBT were assessed and evaluated by the Curtis-Snyder classification[16] and Post classification[17]. Subluxations and dislocations of LBTs were evaluated by Walch's method[18-20].

Lesions of the BPC were assessed and evaluated by the Habermeyer classification[21, 22]. Type was defined as normal; type II was defined as subluxation; and type III was considered dislocation of the LBT, defined as when the LBT was positioned more medially within the EBG than usual[18-20].

Dry unpaired humeri bones

A total of 113 adult intact humeri were collected from skeletons preserved in hermetic boxes by the Department of Anatomy, School of Basic Medicine, Southern Medical University, China.. The age and sex of the donors were unknown. The width, depth, and angles of the EBG were measured (Figure 1B and Figure 2A, 2B).

Images

We retrospectively reviewed 278 images of 3-dimensional (3-D) CT and MRI scans of the shoulder at the Hainan Province Hospital of Traditional Chinese Medicine and the Third Affiliated Hospital of Southern Medical University from January 2016 to January 2020. Criteria for selection were age from 18 to 90 years old; available 3-D CT and MRI scans of the shoulder; and absence of tumor, infection, surgery, or fracture of the shoulder. The mean age of the patients, including 176 males and 102 females, was 56.38±21.27 (18-83) years. The width, depth, and angle of the EBG were measured as above on 3-D CT images (Figure 6B). Lesions of the LBT and BPC were assessed and evaluated as above on MRI scans. Dislocation and subluxation of the LBT were also evaluated on MRI scans.

Classification of the EBG

We classified the intra-articular EBG into 3 types after anatomical observation and refer to the classification system of Welcker and Dierickx[23]. In particular, the intra-articular EBG was classified as either type : with or without a minor synovial sling (Figure 3A); type II: part of the BPC or a hammock-like synovial sling wrapped the intra-articular LBT without an interval or gap (Figure 3B); or type III: the BPC sling wraps the intra-articular LBT with gaps or intervals (Figure 3C).

Consequently, the extra-articular EBG in the lateral view was classified as either type *i*: exhibiting a shape similar to a shaft and in the lateral view appearing as a shaft without narrowing or expanding at the level of turning over the cliff of the lesser tuberosity (Figure 4A, 4B, 4C); type *ii*: having a “sphecidae” shape and in the lateral view girdled by the supratubercular ridge and basal part of greater tuberosity at the level of turning over the cliff of the lesser tuberosity (Figure 4D, 4E, 4F); or type *iii*: with a flare shape and expanded in the lateral view similar to a flare at the level of turning over the cliff of the lesser tuberosity (Figure 4G, 4H, 4I).

The EBG was also classified into 3 types. In particular, the EBG was classified into type *A*: with a U shape, a depth of more than 3-4 mm and a total opening angle that was smaller than 80-90° at the level of turning over the cliff of the lesser tuberosity (Figure 5A, 5B, 5C, 5D); type *B*: with a shallow arc shape, a depth of less than 3-4 mm and a total opening angle that was larger than 80-90° at the level of turning over the cliff of the lesser tuberosity (Figure 5E, 5F, 5G, 5H); or type *C*: with a fishhook shape, a bony spur

that arose from the medial and/or lateral wall of the EBG at the level of turning over the cliff of the lesser tuberosity, and the medial or lateral wall was almost vertical (Figure 5I, 5J, 5K, 5L).

The shape of the articular surface of the humeral head adjacent to the EBG was classified into 2 types. In particular, type *a* was a smooth arc (Figure 6A, 6B, 6C), and type *b* was a wavelike line (Figure 6D, 6E, 6F).

Statistical analysis

All measurements and classifications were independently evaluated by 3 researchers. Interrater agreement was assessed using kappa coefficients as slight, fair, moderate, substantial and almost perfect[24]. All data are presented as the mean±standard deviation. The means of the length, width, depth, and angles were compared among different types by one-way classification ANOVA with SNK *q* or Welch's test with Dunnett's T3 and Dunnett's C tests, as appropriate. Independent samples *t* tests were performed to compare the width, depth and angles between type Ⅰ and type II groups based on the articular surface of the humeral head adjacent to the EBG.. *P* values below 0.05 were considered significant. Statistical analyses were performed using the SPSS 17.0 (SPSS, Inc., Chicago, IL, USA).

Results

Interobserver reliability was substantial or almost perfect

Interobserver kappa values were 0.88 to 0.92 and 0.62 to 0.74 for classification of the intra-articular EBG and extra-articular EBG in the lateral view. The kappa values were 0.79 to 0.93 for classification of the EBG in the superoinferior view into types *A*, *B* and *C* and 0.80 to 0.93 for classification of the shape of the articular surface of the humeral head adjacent to the EBG. These data indicated substantial or almost perfect reliability across the 3 observers.

Measurement and classification distribution of the EBG in cadaveric specimens

The length, width, depth, medial wall angle and total open angle of the EBG in cadaveric specimens are presented in Table 1. The classification distributions of the EBG are presented in Table 2. Lesions of the LBT were found in 2 specimens: one type Ⅰ lesion (Figure 7A) and one type II lesion (Figure 7B) based on the Curtis-Snyder classification[16], and one small tear (Figure 7A) and 1 medium tear (Figure 7B) based on the Post classification[17]. There were 2 subluxations among all 34 type *B* LBTs, and no dislocations of the LBT were found (Figure 7B, 7C, 7D). Consequently, only 2 lesions of the BPC, one type Ⅰ (Figure 8A) and one type II lesion (Figure 8B, 8C), were detected based on the Habermeyer classification[21, 22]. Both injured LBTs were subluxated and were type *B* and type *C*; meanwhile, both injured LBTs were type Ⅰ and type *iii* EBGs (Figure 7A, 7B). No mesotendon of the LBT was found within the EBG.

Distribution of EBG classifications in dry humeri

The distribution of EBG classifications in dry humeri are presented in Table 3 and Figure 9. For EBG classifications in the superoinferior view, most humeri were type *A* with a "U" shape (81/113, 73.45%),

while few were type *C* with a “fishhook” shape (10/113, 8.85%) (Figure 5). Meanwhile, for classifications in the lateral view, most humeri were type *ii* with a “sphecidae” shape (57/113, 50.44%), while few were type *iii* with a “flare” shape (14/113, 12.39%) (Figure 4). Regarding the articular surface of the humeral head adjacent to the EBG, most humeri were type *b* with wavelike lines (71/113, 62.83%), while few were of type *a* with smooth arcs (42/113, 37.17%) (Figure 6).

Measurement of the EBG and its relationship with classification in the dry humeri

The width, depth, medial wall angle and total open angle of the EBG in the dry humeri are presented in Table 4. The total open angle was the largest (F=63.52; P<0.001) and the depth and medial angle were the smallest (F=79.59 and 36.37, respectively; both P<0.001) in type *B*, and type *C* had the smallest width (F=5.34, P=0.006). Additionally, the depth and medial angle were largest (F=16.89 and 5.85; P<0.001 and P=0.004, respectively) and the total open angle was the smallest in type *ii* (F=10.82, P<0.001). The width, depth, medial wall angle and total open angle of the EBG in dry the humeri were not significantly different between the 2 types classified based on the articular surface adjacent to the EBG (t=0.53, 0.68, 0.87, and 0.87; all P≥0.39).

Distribution of EBG classifications based on 3-D CT

The distributions of EBG classifications based on 3-D CT are presented in Table 5 and Figure 10. Nearly half of the classifications were type *ii* with a “sphecidae” shaped (134/278, 48.20%) EBG, while few were type *iii* with a “flare” shape (24/278, 8.63%) (Figure 4). Meanwhile, most were type *A* with a "U" shape (176/278, 63.31%), while few were type *C* with a “fishhook” shape (29/278, 10.43%) (Figure 5). Regarding the articular surface of the humeral head adjacent to the EBG, most classifications were type *b* with wavelike lines (166/278, 59.71%), while few were type *a* with smooth arcs (112/278, 40.29%) (Figure 6).

Measurement of the EBG and the distribution based on the classification of images

Data on the width, depth, and angles in the images are presented in Table 6. The width and total open angle were the largest (F=280.75 and 538.56, respectively; both P<0.001) and the depth and medial angle were the smallest (F=18.63 and 85.25, respectively; both P<0.001) in type *B*. Additionally, the depth and medial angle were the smallest (F=30.10 and 18.74, respectively; both P<0.001) and the width and total open angle were the largest (F=14.93 and 27.14; both P<0.001) in type *iii*. The width, depth, medial wall angle and total open angle of the EBG in the images were not significantly different among the types based on classification of the articular surface adjacent to the EBG (t=0.14, 0.44, 0.68, and 0.63, respectively; all P≥0.50).

Lesions of the LBT and BPC on MRI and their correlations with classifications

The distributions of the LBT and BPC lesions on MRI are presented in Table 6 and Figure 10. Most LBT locations within the EBG were normal (261/278, 93.88%) (Figure 7E), with 13 subluxations (Figure 7F) and 4 dislocations (Figure 7G). Interestingly, all of the subluxations and dislocations occurred in type *B*, and most lesions of the LBT and BPC occurred in type *B* (61/120, 50.83%; 65/117, 55.56%, respectively)

(χ^2=16.55 and 26.05; both *P*<0.001). Meanwhile, most lesions were type according to the Curtis-Snyder classification (90/121, 74.38%) and type II according to the Post classification (61/121) (Table 5). Most BPC lesions were type II (78/117, 66.67%), while few were type III (7/117, 5.98%) (χ2=110.80; *P*<0.001) (Figure 8). Notably, the LBT was injured in 83.56% of type *B* and 100% of type *C* EBGs (χ2=135.69, *P*<0.001), which warrants further investigation. In addition, the LBT was injured in 95.83% of type *iii* EBGs (χ2=31.89, *P*<0.001). Similarly, the BPC was injured in 89.04% of type *B* and 93.10% of type *C* EGBs (χ2=153.14, *P*<0.001), while the BPC was injured in 95.8% of type *iii* EBGs (χ2=33.79, *P*<0.001).

Discussion

Many studies have mentioned the EBG[17, 25–31], but they did not define the EBG by rule and line. Many studies on tenodesis of the LBT valued a location 10 mm distal to the proximal EBG that anatomically lies superior to the pectoralis major tendon[25, 26, 30]. Moreover, the point or segment of the EBG varied among studies based on the perspective from the schematic diagram[17, 30, 32]. As the segment of the EBG is very important for shoulder pathology, physical examinations and surgical operations, we believe that it is necessary to accurately define the EBG. We defined the EBG as an anatomic and functional segment along the LBT from the upper margin of the transverse humeral ligament to the intra-articular soft tissue surrounding the LBT adjacent to the entrance of the capsule (Fig. 1A). The EBG is divided into two parts: an intra-articular segment and an extra-articular segment. Usually, the point of the upper margin of the transverse humeral ligament is the turning point over a cliff of the lesser tuberosity (Fig. 1A, 1B).

The dimensions and morphology of the intertubercular sulcus are involved in LBT lesions[14, 33] [34], although there are still many controversies[10, 21]. Lesions of the LBT create three types of bony abnormalities within the intertubercular sulcus: rotator cuff calcifications, medial and lateral spurs (small bony excrescences), and degenerative changes[14, 33]; bony abnormalities are considered to be correlated with lesions of the LBT as a matter of course. We found that type *C* of the EBG classification in the superoinferior view correlated with LBT lesions. The groove was designated as narrow, normal, or shallow based on mean measured opening angles of less than 66°, 94°, and 118°, respectively[10, 35], and the morphometry of the bicipital groove on MRI had no correlation with lesions of the intra-articular LBT[10]. However, we speculated that the EBG rather than the middle segment of the bicipital groove may be more clinically significant. Previous studies may have drawn different conclusions based on measurements of different segments of the bicipital groove. In our study, all subluxations or dislocations were distributed in type *B* based on the EBG classification in the superoinferior view, both in cadavers and images.

Lesions of the LBT and BPC are considered to be associated with shoulder pain. The supratubercular ridge, which increases mechanical wear and tear[33], could increase the instability of the LBT within the EBG and thus favor disease of the LBT[33]. The LBT may dislocate and slide over the lesser tuberosity if the anterior supporting structures are torn and the medial wall itself is deficient[13]. We classified the EBG into different types based on anatomical variations of the bony landmarks. The extra-articular segment

of the EBG, which is a semiosseous channel, was classified into 3 types in the lateral view and 3 types in the superoinferior view. Additionally, the articular surface near the EBG was classified into 2 types. Most LBT and BPC lesions were found in type II and type III EBGs based on the classification in the lateral view. Some studies have considered that the supratubercular ridge may predispose patients to LBT dislocation[13, 33, 36], and our data supported the notion that the supratubercular ridge might correlate with pathology. To our surprise, bony spurs arising from the wall of the intertubercular sulcus (EBG) at the level of the upper margin of the transverse humeral ligament, which belonged to type *iii*, did not appear to be a protective sign but rather a sign of LBT lesions (Fig. 5). Osseous spurs seemed to correlate with lesions of the LBT and BPC.

The types of articular surface near the EBG did not seem to correlate with any lesion of the LBT or BPC. A type *b* articular surface near the EBG was most common, and this type may be a helpful sign indicating the direction of the LBT under shoulder arthroscopy. Classification of the intra-articular EBG may be practically useful to evaluate the type and lesion of the BPC under shoulder arthroscopy. Both lesions of the LBT were type I, which meant that the soft tissue wrapping of the LBT might protect the LBT rather than serving as the origin of biceps-related complaints[23]. No mesotendon of the LBT was found within the EBG, which meant that the LBT lacked nutrient vessels in this segment.

Importantly, the images for this retrospective analysis were collected from patients with shoulder disorders; therefore, the numbers of lesions and injuries of the LBT and BPC were much higher than those in the general population. Our hypothesis and speculative conclusion based on anatomical and imaging observations and measurements require further investigation. The greatest possible limitation was the lack of arthroscopic verification and study. By clarifying the concept, location and classification of the EBG, we hope to gain better insight into the relationships between variations in the EBG and peripheral tissue injury, which should be the subject of further anatomical and clinical research.

Conclusion

In this work, we defined the EBG and examined the morphological parameters, classifications, and their relationships with lesions of the LBT and BPC through an anatomic and imaging study. The EBG is an anatomical concept worthy of clinical attention. Anatomical variations in the EBG correlated with lesions of the LBT and BPC.

Declarations

Funding

This work was funded by Guangdong Basic and Applied Basic Research Foundation (No.2020A151501998).

Disclaimer

No financial biases exist for any author and their immediate families from any commercial entity related to the subject of this article.

Approval of Institutional Review Board: The research was examined and approved by the Medical Ethics Committee of Hainan Province Hospital of Traditional Chinese Medicine (approval number: 2020015) and Human Research Ethics Committee of the Third Affiliated Hospital of Southern Medical University (approval number: 2020-015-003).

References

1. Raynor MB, Kuhn JE. Utility of features of the patient's history in the diagnosis of atraumatic shoulder pain: a systematic review. J SHOULDER ELB SURG. 2016;25(4):688–94.
2. Roberts AM, Peters TJ, Brown KR. New light on old shoulders: palaeopathological patterns of arthropathy and enthesopathy in the shoulder complex. J ANAT. 2007;211(4):485–92.
3. Theopold J, Marquaß B, Fakler J, Steinke H, Josten C, Hepp P. The bicipital groove as a landmark for reconstruction of complex proximal humeral fractures with hybrid double plate osteosynthesis. BMC SURG. 2016;16:10.
4. Singh R, Singla M, Tubbs RS. Macro/micro observational studies of fibres maintaining the biceps brachii tendon in the bicipital groove: application to surgery, pathology and kinesiology. FOLIA MORPHOL. 2015;74(4):439–46.
5. MacDonald K, Bridger J, Cash C, Parkin I. Transverse humeral ligament: Does it exist? CLIN ANAT. 2007;20(6):663–7.
6. Kwon YW, Hurd J, Yeager K, Ishak C, Walker PS, Khan S, Bosco RJA, Jazrawi LM: **Proximal biceps tendon–a biomechanical analysis of the stability at the bicipital groove**. *Bulletin of the NYU hospital for joint diseases* 2009, **67**(4):337.
7. Urita A, Funakoshi T, Amano T, Matsui Y, Kawamura D, Kameda Y, Iwasaki N. Predictive factors of long head of the biceps tendon disorders—the bicipital groove morphology and subscapularis tendon tear. J SHOULDER ELB SURG. 2016;25(3):384–9.
8. Refior HJ, Sowa D. Long tendon of the biceps brachii: Sites of predilection for degenerative lesions. J SHOULDER ELB SURG. 1995;4(6):436–40.
9. Pfahler M, Branner S, Refior HJ. The role of the bicipital groove in tendopathy of the long biceps tendon. J SHOULDER ELB SURG. 1999;8(5):419–24.
10. Abboud JA, Bartolozzi AR, Widmer BJ, DeMola PM. Bicipital groove morphology on MRI has no correlation to intra-articular biceps tendon pathology. J SHOULDER ELB SURG. 2010;19(6):790–4.
11. Gleason PD, Beall DP, Sanders TG, Bond JL, Ly JQ, Holland LL, Pasque CB. The Transverse Humeral Ligament. The American Journal of Sports Medicine. 2017;34(1):72–7.
12. Tamborrini G, Möller I, Bong D, Miguel M, Marx C, Müller A, Müller-Gerbl M. The Rotator Interval - A Link Between Anatomy and Ultrasound. Ultrasound international open. 2017;3(3):E107–16.

13. Levinsohn EM, Santelli ED. Bicipital groove dysplasia and medial dislocation of the biceps brachii tendon. SKELETAL RADIOL. 1991;20(6):419–23.
14. Cone RO, Danzig L, Resnick D, Goldman AB. The bicipital groove: radiographic, anatomic, and pathologic study. AJR Am J Roentgenol. 1983;141(4):781–8.
15. Wafae N, Atencio Santamaría LE, Vitor L, Pereira LA, Ruiz CR, Wafae GC. Morphometry of the human bicipital groove (sulcus intertubercularis). J SHOULDER ELB SURG. 2010;19(1):65–8.
16. Curtis A, Snyder S. Evaluation and treatment of biceps tendon pathology. The Orthopedic clinics of North America. 1993;24(1):33–43.
17. Toshiaki A, Itoi E, Minagawa H, Yamamoto N, Tuoheti Y, Seki N, Okada K, Shimada Y. Cross-sectional area of the tendon and the muscle of the biceps brachii in shoulders with rotator cuff tears. ACTA ORTHOP. 2009;76(4):509–12.
18. Walch G, Nove-Josserand L, Boileau P, Levigne C. Subluxations and dislocations of the tendon of the long head of the biceps. J Shoulder Elbow Surg. 1998;7(2):100–8.
19. Koh K, Kim SC, Yoo JC. Arthroscopic Evaluation of Subluxation of the Long Head of the Biceps Tendon and Its Relationship with Subscapularis Tears. Clin Orthop Surg. 2017;9(3):332.
20. Jeong JY, Park SM, Park YE, Yoo JC. Morphological classification of anatomical variants of the intra-articular portion of the long head of the biceps brachii tendon and analysis of the incidence and the relationship with shoulder disease for each subtype. J ORTHOP SURG-HONG K. 2017;25(3):920333708.
21. Nakata W, Katou S, Fujita A, Nakata M, Lefor A, Sugimoto H. Biceps pulley: normal anatomy and associated lesions at MR arthrography. Radiographics: a review publication of the Radiological Society of North America Inc. 2011;31(3):791–810.
22. Hawi N, Liodakis E, Garving C, Habermeyer P, Tauber M. Pulley lesions in rotator cuff tears: prevalence, etiology, and concomitant pathologies. ARCH ORTHOP TRAUM SU. 2017;137(8):1097–105.
23. Dierickx C, Ceccarelli E, Conti M, Vanlommel J, Castagna A. Variations of the intra-articular portion of the long head of the biceps tendon: a classification of embryologically explained variations. J SHOULDER ELB SURG. 2009;18(4):556–65.
24. Yuan S, Zou Y, Li Y, Chen M, Yue Y. A clinically relevant MRI grading system for lumbar central canal stenosis. Clin Imaging. 2016;40(6):1140–5.
25. Müller S, Flury R, Zimmermann S, de Wild M, Fogerty S, Lafosse L, Bongiorno V, Rosso C. The new LassoLoop360° technique for biomechanically superior tissue grip. Knee Surg Sports Traumatol Arthrosc. 2019;27(12):3962–9.
26. Kerschbaum M, Alt V, Pfeifer C. The All-Inside Arthroscopic Loop Tenodesis Procedure to Treat Long Head of Biceps Tendon Pathologies. Arthroscopy Techniques. 2019;8(12):e1551–4.
27. Narvani AA, Atoun E, Van Tongel A, Sforza G, Levy O. The “Anchor Shape” Technique for Long Head of the Biceps Tenotomy to Avoid the Popeye Deformity. Arthroscopy Techniques. 2013;2(2):e167–70.

28. Buck FM, Dietrich TJ, Resnick D, Jost B, Pfirrmann CWA. Long biceps tendon: normal position, shape, and orientation in its groove in neutral position and external and internal rotation. RADIOLOGY. 2011;261(3):872–81.
29. Mazaleyrat M, Barthélémy R, Bouilleau L, Charousset C, Berhouet J. **Inter- and intra-observer reproducibility of ultrasound analysis of the long head of the biceps**. *Orthopaedics & Traumatology: Surgery & Research* 2020.
30. Patzer T, Rundic JM, Bobrowitsch E, Olender GD, Hurschler C, Schofer MD. Biomechanical Comparison of Arthroscopically Performable Techniques for Suprapectoral Biceps Tenodesis. Arthroscopy: The Journal of Arthroscopic Related Surgery. 2011;27(8):1036–47.
31. Valenti P, Benedetto I, Maqdes A, Lima S, Moraiti C. “Relaxed” Biceps Proximal Tenodesis: An Arthroscopic Technique With Decreased Residual Tendon Tension. Arthroscopy Techniques. 2014;3(5):e639–41.
32. Patzer T, Santo G, Olender G, Wellmann M, Hurschler C, Schofer M. Suprapectoral or subpectoral position for biceps tenodesis: biomechanical comparison of four different techniques in both positions. J SHOULDER ELB SURG. 2012;21(1):116–25.
33. Ueberham K, Le Floch-Prigent P. Intertubercular sulcus of the humerus: biometry and morphology of 100 dry bones. SURG RADIOL ANAT. 1998;20(5):351–4.
34. Neviaser R. Lesions of the biceps and tendinitis of the shoulder. The Orthopedic clinics of North America. 1980;11(2):343–8.
35. Smith AL. **Morphologic classification of the bicipital groove**. In: *Proceedings of the Annual Meeting of the American Academy of Orthopaedic Surgeons (AAOS '07).* SanDiego,California, USA.
36. Rajan YS, Kumar SKS. Morphometric Study on Bicipital Groove among South Indian Population. Journal of clinical diagnostic research: JCDR. 2016;10(7):C1–3.

Tables

Table 1 Measurement of EBG in cadavers for different classifications

classification		length	depth	width	total open angle	medial angle
total		14.26±8.46*	4.97±0.89	7.80±1.18	74.26±14.12	55.23±9.37
intra-articular EBG	type	6.86±0.50*	5.05±0.90	7.72±1.15	74.29±14.16	53.94±9.02
	type	14.18±3.79*	4.79±0.99	7.72±0.92	74.86±15.69	55.03±10.51
	type	30.85±5.41	5.06±0.63	8.64±1.80	72.01±9.41	58.82±5.58
EBG in lateral view	type	14.45±8.97	5.24±0.66	8.06±1.47	68.29±7.08	57.03±5.37
	type	14.15±8.88	4.80±0.97	7.73±1.01	74.51±14.15	55.16±14.15
	type	7.54	3.78	8.3	112.3	37.3
EBG in superoinferior view	type	14.79±9.14	5.16±0.57	7.79±1.25	70.24±7.51	57.17±5.23
	type	11.63±2.69	3.28±0.38	8.01±0.51	97.25±15.63	39.73±5.88
	type	12.18±6.55	4.74±1.36	8.45±0.21	84.50±39.32	59.20±30.97
cartilaginous surface	type	15.46±7.55	4.56±0.94	7.76±1.01	75.47±17.46	52.72±11.91
	type	13.31±9.22	5.19±0.79	7.93±1.28	73.30±11.23	57.22±6.43

Table 2 Distribution of different types of classifications and lesions in cadavers

classification		type	type	type	type
intra-articular EBG		11	18	5	
in lateral view of EBG		10	23	1	
in superoinferior view of EBG		28	4	2	
cartilaginous surface		15	19		
lesions of LTB	Curtis-Snyder	1	1	0	0
	Post	1	1	0	
lesions of BPC		1	1	0	0
location of LTB within EBG		31	2	0	

Table 3 Distribution of different types of classifications in dry humeri

classification	type	type	type	χ^2	*p*
in superoinferior view	81	22	10	76.69	0.001
in lateral view	42	57	14	25.29	<0.001
cartilaginous surface	42	71		7.44	0.006

Table 4 Measurement of EBG for different classifications in dry humeri

classification		depth	width	total open angle	medial angle
total		4.06±0.74	7.76±1.28	72.83±25.97	56.61±16.19
in superoinferior view	type □	4.33±0.46▲	7.77±1.15▲	67.92±18.96	58.41±12.70
	type □	2.92±0.43	8.20±1.59▲	107.12±16.02	39.69±9.37
	type □	4.45±0.68▲	6.66±1.05	37.21±10.18	79.25±18.03
in lateral view	type □	3.79±0.70*	7.94±1.36*	79.90±22.64*	52.46±13.27*
	type □	4.41±0.50	7.56±1.17*	63.04±19.19	61.47±14.37
	type □	3.49±0.97*	7.99±1.45*	91.48±40.70*	49.28±24.45*
cartilaginous surface	type □	4.02±0.71□	7.86±1.31□	75.60±21.19□	57.73±14.74□
	type □	4.09±0.75□	7.69±1.27□	71.20±28.45□	55.95±17.06□

Table 5 Distribution of different types of classifications and lesions in images

classification		type □	type □	type □	type □
in superoinferior view of EBG		176	73	29	
in lateral view of EBG		120	134	24	
cartilaginous surface		112	166		
lesions of LTB	Curtis-Snyder	90	25	3	2
	Post	49	61	10	
lesions of BPC		19	78	7	13
location of LTB within EBG		261	13	4	

Table 6 Measurement of EBG for different classifications in images

classification		depth	width	total open angle	medial angle
total		3.99±0.76	7.97±1.24	75.34±17.07	56.08±13.06
in superoinferior view	type	4.33±0.38▲	7.93±1.20	71.52±8.16	59.82±11.45
	type	2.95±0.39	8.47±1.17	96.87±6.70	42.97±6.71
	type	4.49±0.50▲	6.92±0.86	44.35±7.38	56.08±13.06
in lateral view	type	4.10±0.65*	7.88±1.15*	72.51±15.90*	58.57±12.35*
	type	4.07±0.76*	7.82±1.20*	73.87±16.46*	56.42±12.90
	type	2.94±0.39	9.22±1.24	97.34±7.41	41.78±7.56
cartilaginous surface	type	3.99±0.75	7.93±1.00	76.16±14.93	55.48±12.83
	type	3.98±0.77	7.99±1.37	74.79±18.38	56.48±13.24

Figures

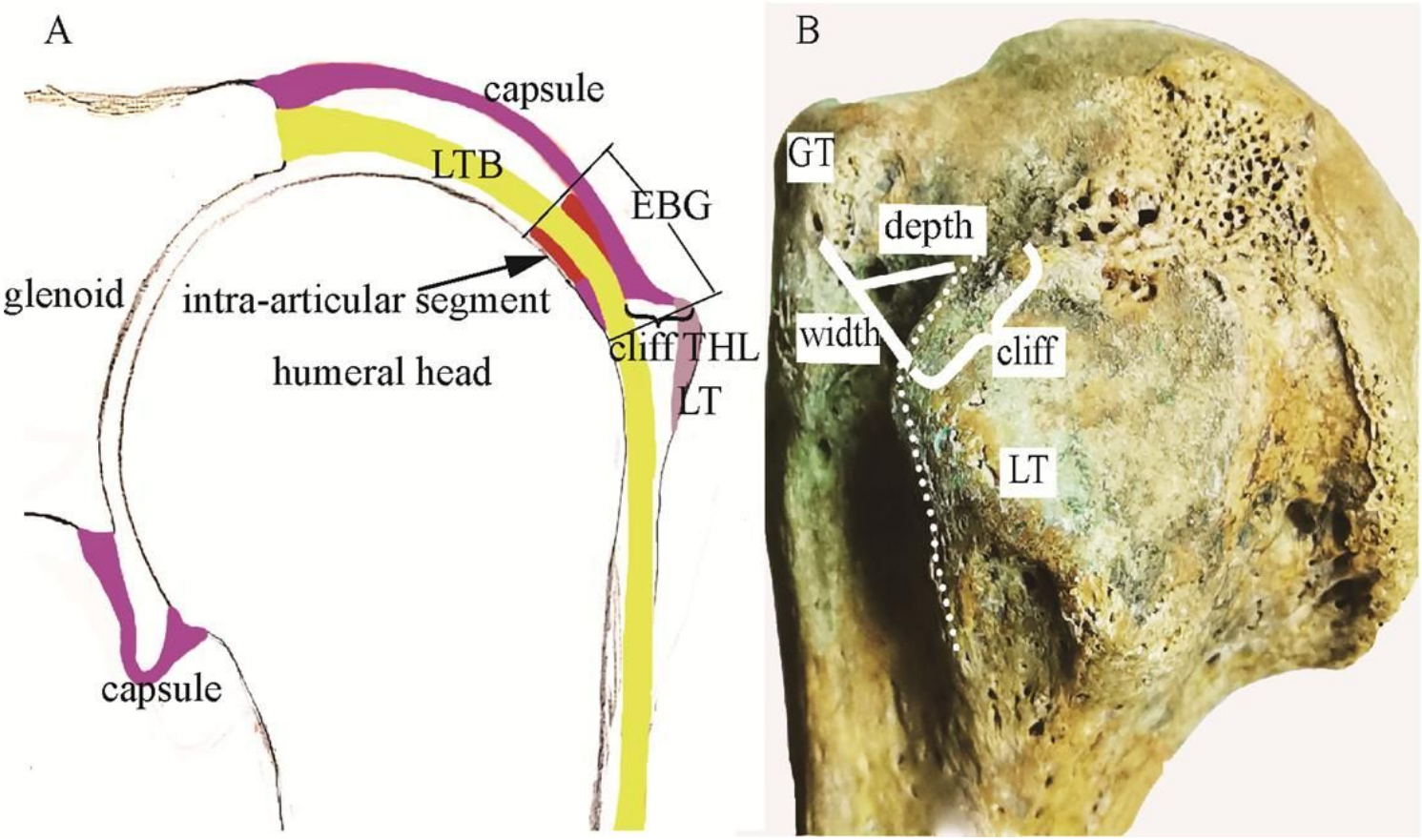

Figure 1

Overview of the EBG and its adjacent anatomical structures. (A) Schematic of the morphology of the anatomy through the LBT in the coronal view showing the EBG and its adjacent anatomical structures. The EBG is a channel with a variable length and a constant position that consists of two parts: an intra-articular segment (red) and an extra-articular segment. (B) Photograph of a dry humerus showing that the cliff of the lesser tubercles is steep as well as measurements of the EBG.

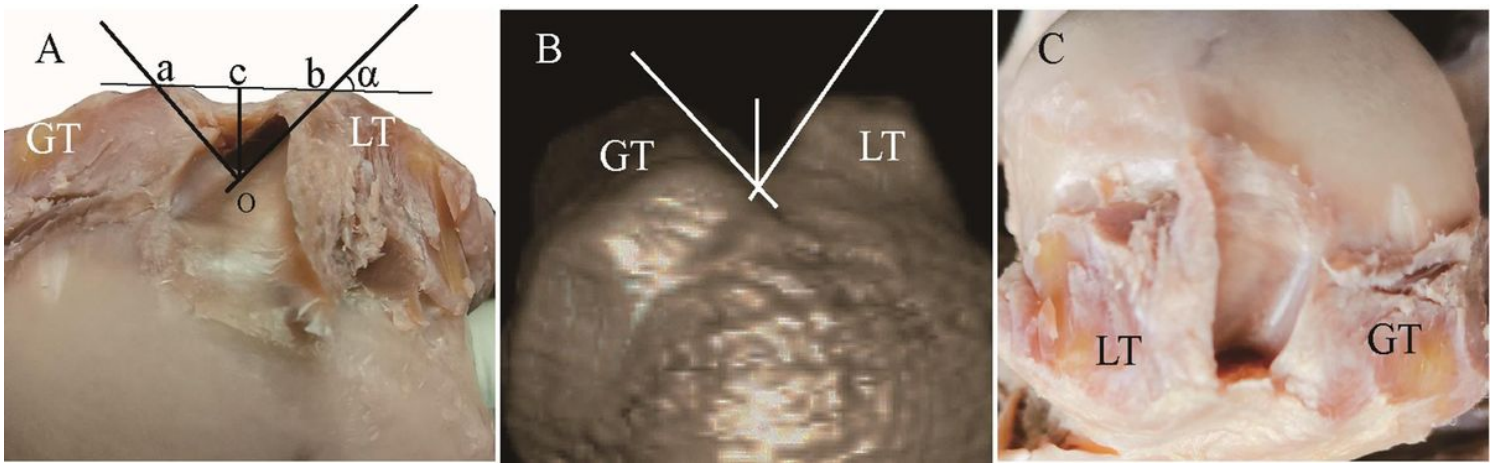

Figure 2

Measurement of the length, depth, width, medial wall angles and total open angle of the EBG. (A) Measurement of the depth, width, medial wall angle and total open angle of the EBG on a cadaver. (B) Measurement of the depth, width, medial wall angle and total open angle of the EBG on 3-D CT. (C) Measurement of the length of the EBG on a cadaver.

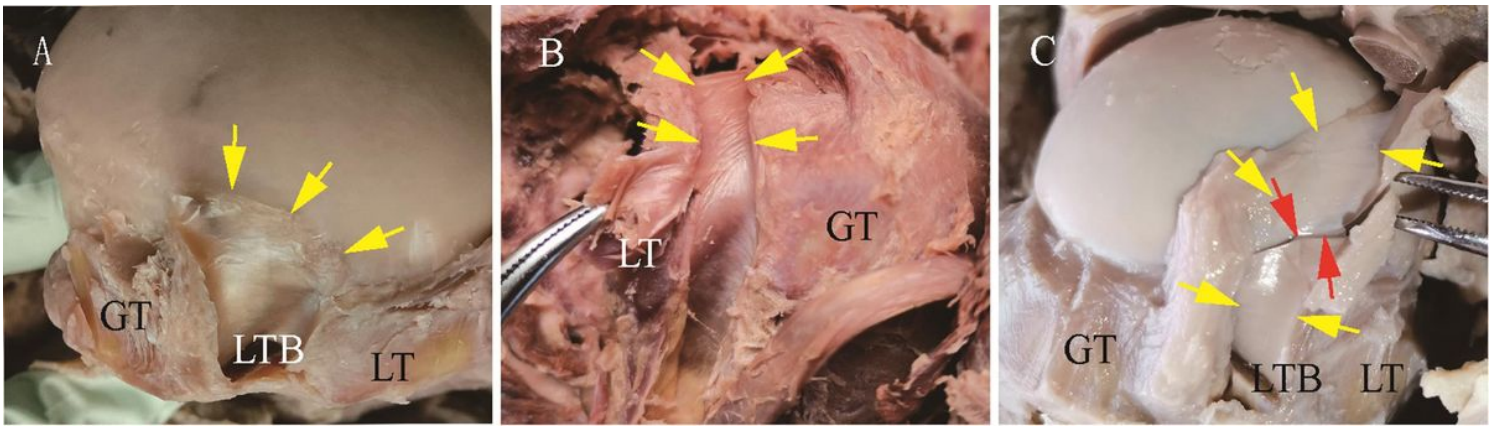

Figure 3

Photograph of cadavers showing the 3 types of intra-articular segments of the EBG (yellow arrow). (A) Type Ⅰ: without or with a minor synovial sling. (B) Type II: part of the BPC or a hammock-like synovial sling wraps the intra-articular LBT without an interval or a gap. (C) Type III: the BPC sling wraps the intra-articular LBT with gaps or intervals (red arrow).

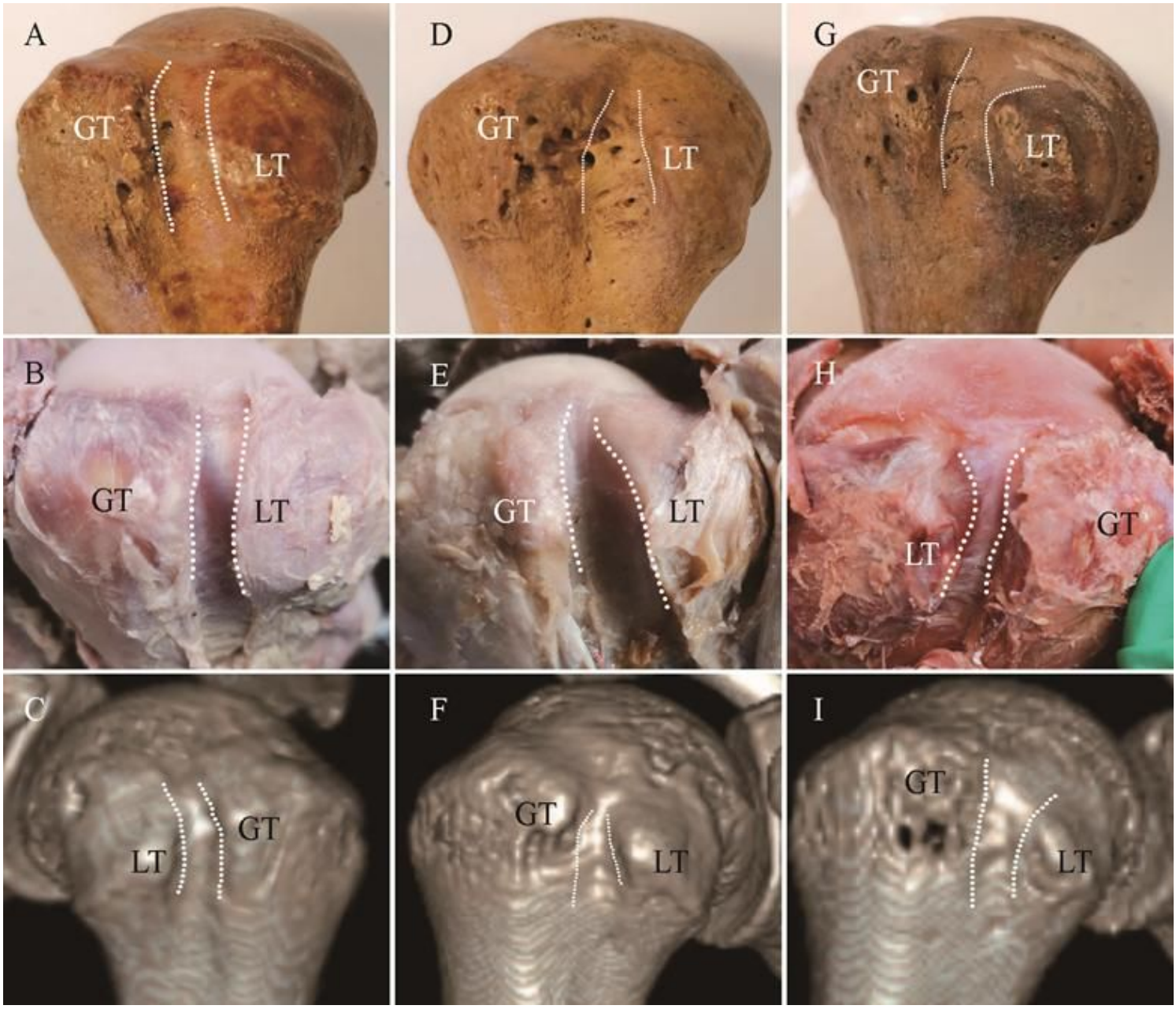

Figure 4

Dry humerus, antiseptic cadaver and 3-D CT images showing the classifications of 3 types of extra-articular segments of the EBG in the lateral view. (A, B, C) Type i: a shaft shape; the extra-articular EBG in the lateral view appears as a shaft without narrowing or expansion. (D, E, F) Type ii: a sphecidae shape; the extra-articular EBG in the lateral view is girdled by the supratubercular ridge and basal part of the greater tubercle. (G, H, I) Type iii: a flare shape; the extra-articular EBG in the lateral view expands similar to a flare.

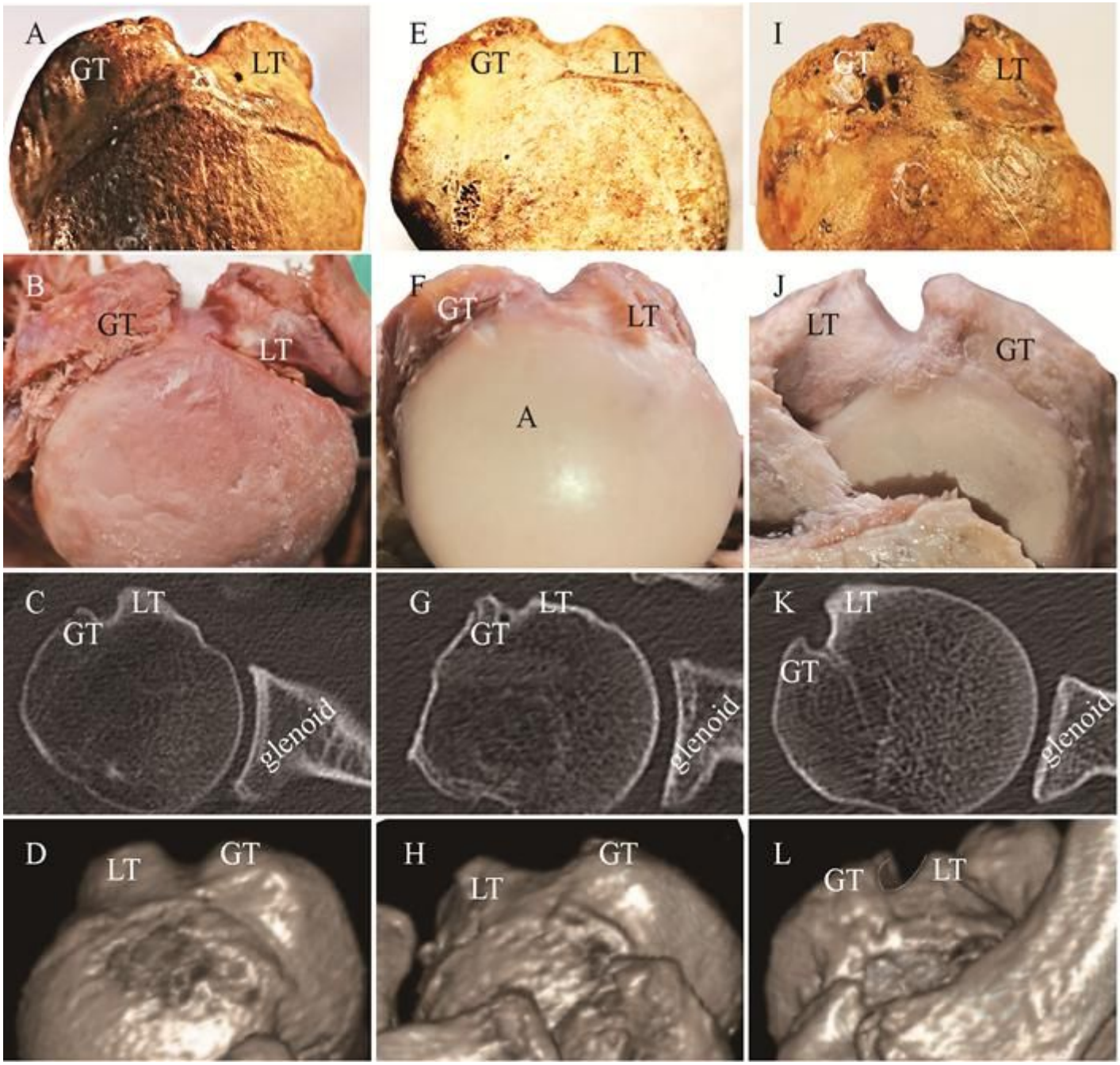

Figure 5

Dry humerus, antiseptic cadaver and CT images showing the classifications of 3 types of extra-articular segments of the EBG in the superoinferior view. (A, B, C, D) Type A: a U shape; the depth is greater than 3-4 mm and the total opening angle is smaller than 80-90°. (E, F, G, H) Type B: a shallow arc shape; the depth is less than 3-4 mm and the total opening angle is larger than 80-90°. (I, J, K, L) Type C: a fishhook shape; bony spurs arise from the medial and/or lateral wall of the EBG at the level of the upper margin of the transverse humeral ligament, and the medial or lateral wall is almost vertical.

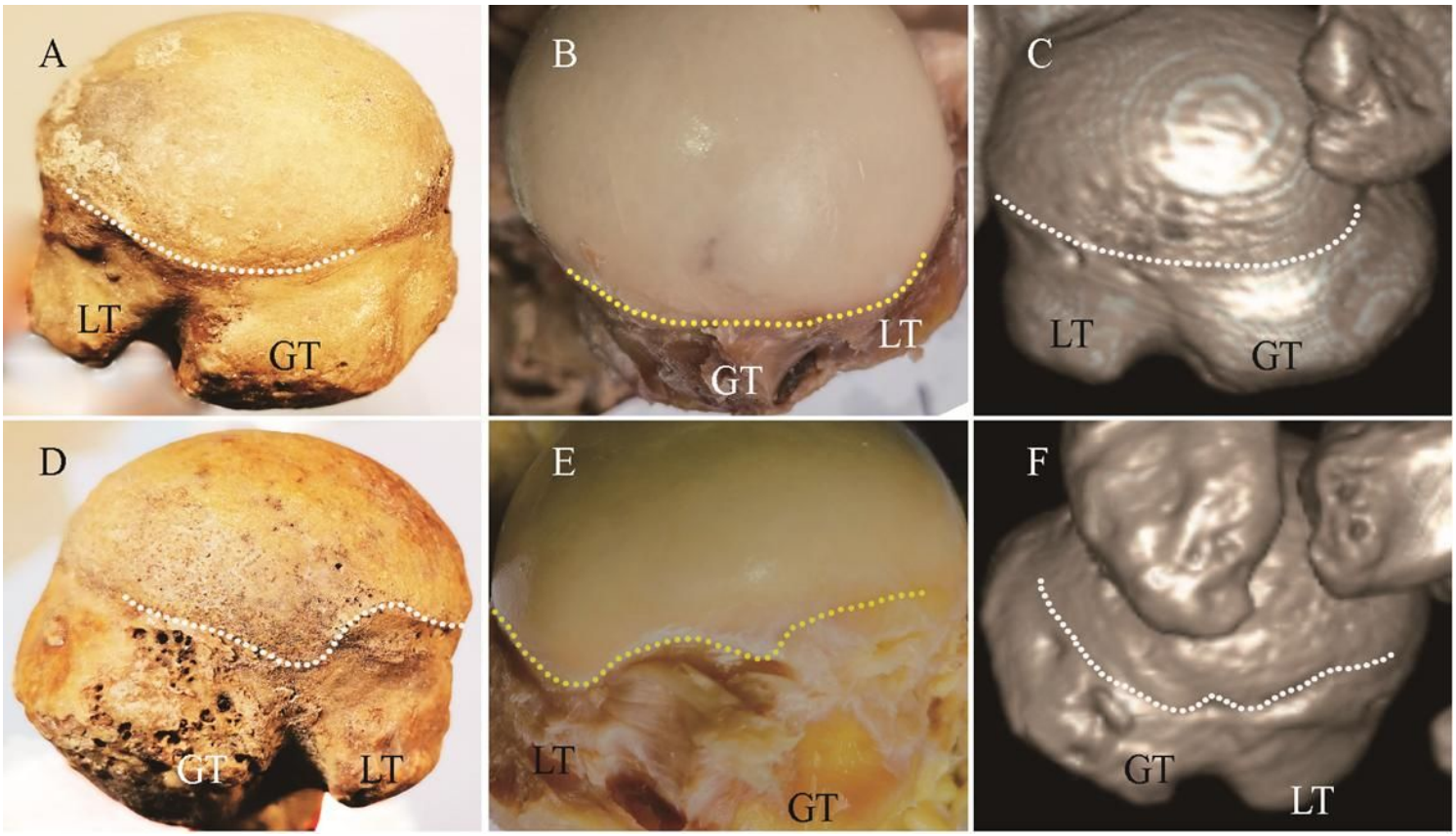

Figure 6

Dry humerus, cadaver and CT images showing the classification of 2 types of articular surfaces of the humeral head adjacent to the EBG. (A, B, C) Type a: smooth arc. (D, E, F) Type b: wavelike line.

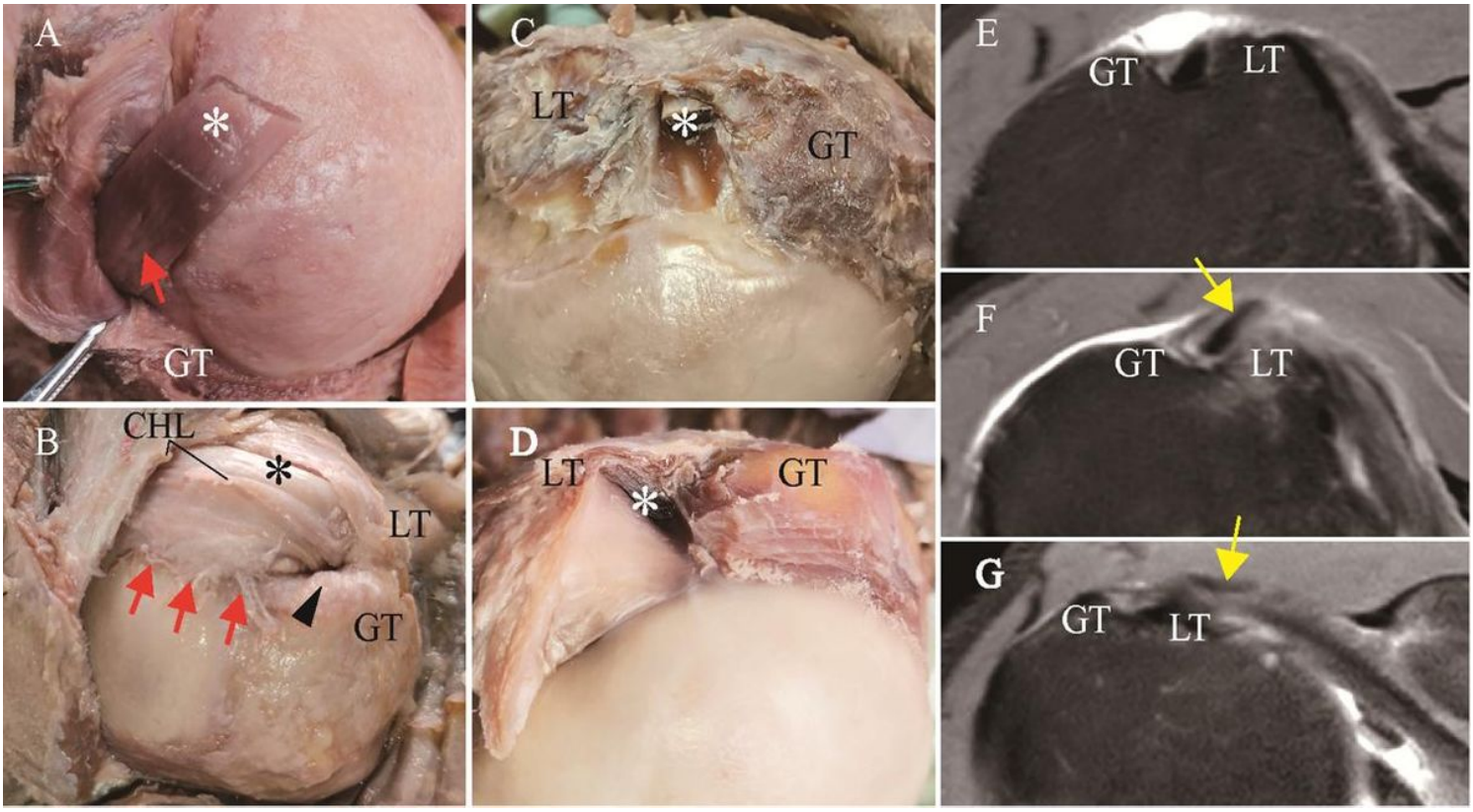

Figure 7

Locations and lesions of the long head of the biceps brachii tendon (LBT). (A) A type I LBT based on the Curtis-Snyder classification and on the Post classification in an antiseptic cadaver (red arrow). (B) The injured LBT presents as type II based on the Curtis-Snyder classification and as type II based on the Post classification in an antiseptic cadaver (red arrow). Spurs arise from the lateral wall of the EBG (black head of arrow), and the LBT is subluxated in an antiseptic cadaver (*). (C) The location of the LBT is normal without subluxation or dislocation (*). (D) The LBT is subluxated in an antiseptic cadaver (*). (E) The location of the LBT is normal on MRI. (F) The LBT is subluxated on MRI (yellow arrow). (G) The LBT is dislocated on MRI (yellow arrow).

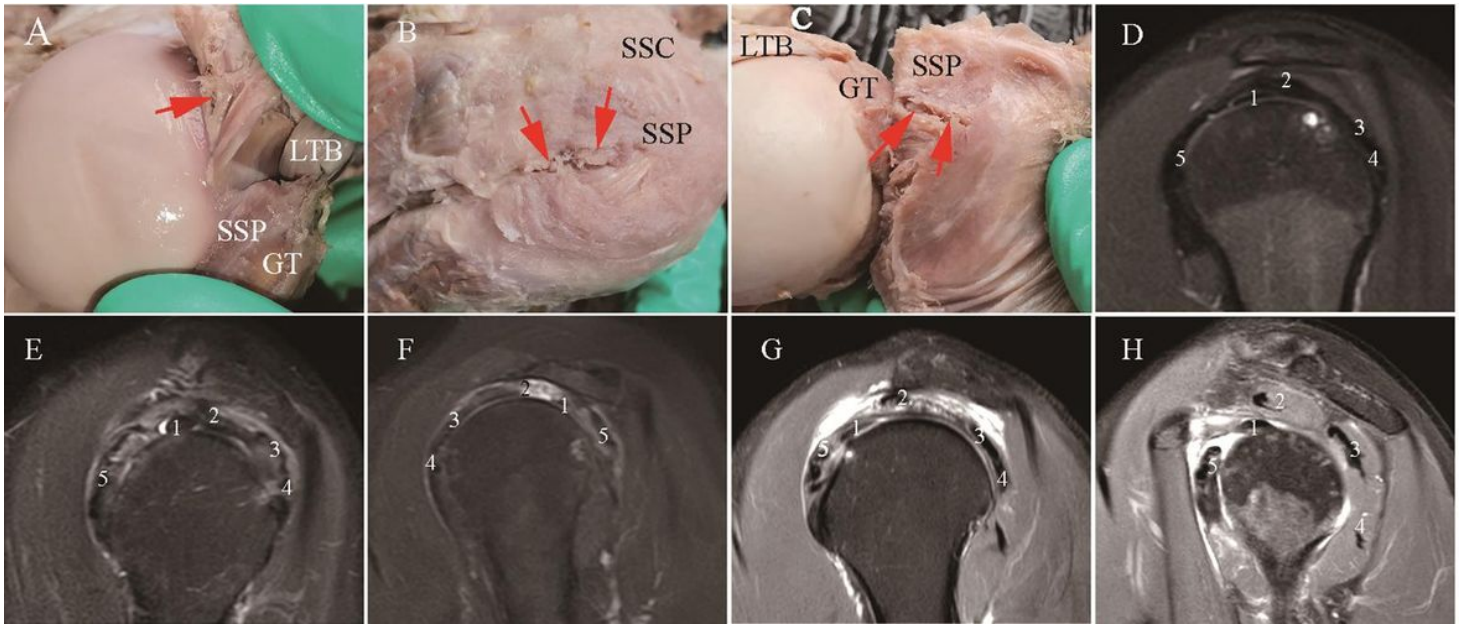

Figure 8

Lesion of the biceps pulley complex (BPC). (A) Photograph of antiseptic cadavers showing a type I lesion of the BPC based on the Habermeyer classification (red arrow). (B, C) Photograph of antiseptic cadavers showing a type II lesion of the BPC based on the Habermeyer classification (red arrow). (D) MRI showing the normal structures of the BPC. (E) MRI showing a type I BPC lesion. (F) MRI showing a type II BPC lesion. (G) MRI showing a type III BPS lesion. (H) MRI showing a type IV BPC lesion.

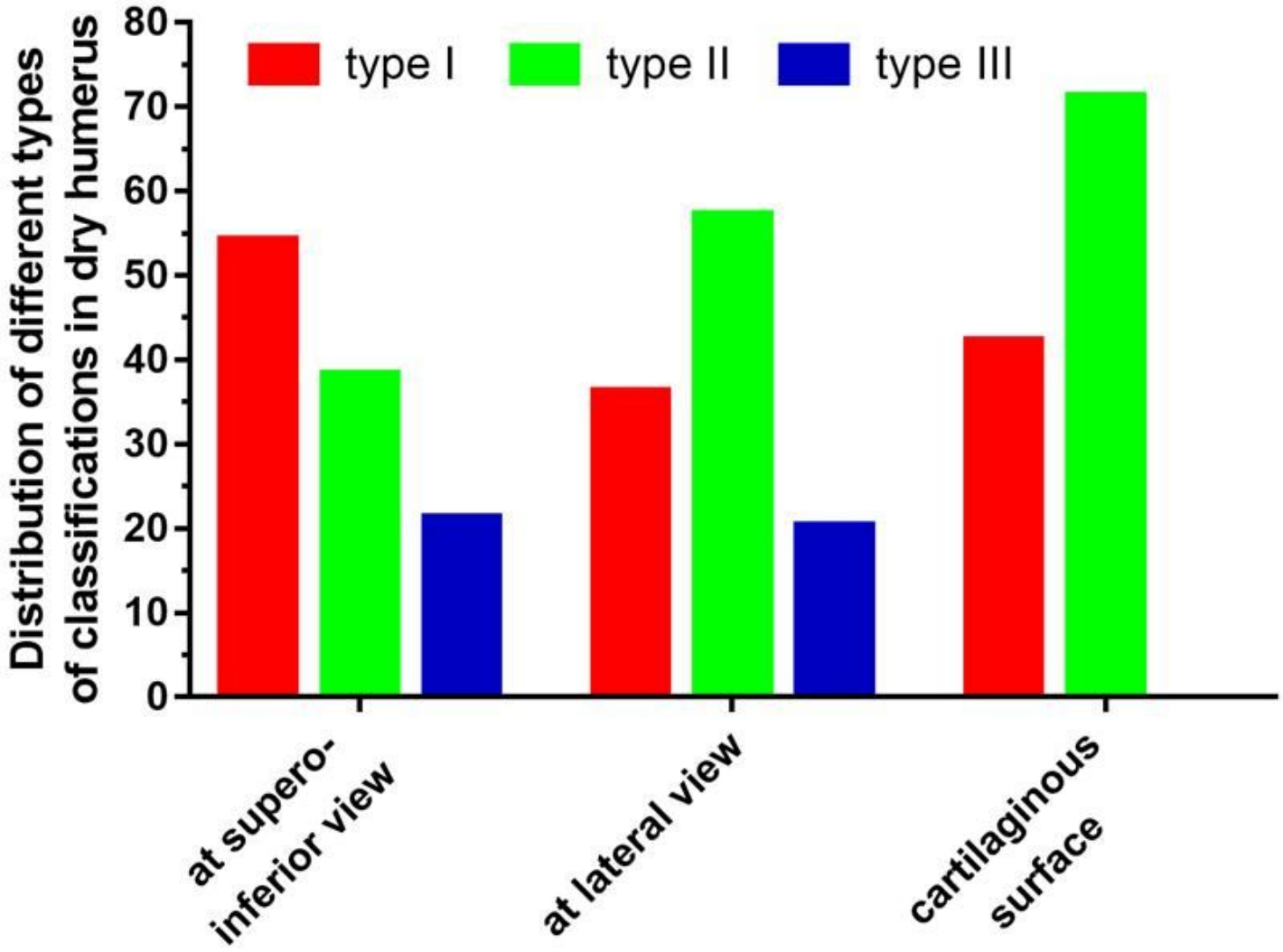

Figure 9

Distribution of different classification types in dry humeri.

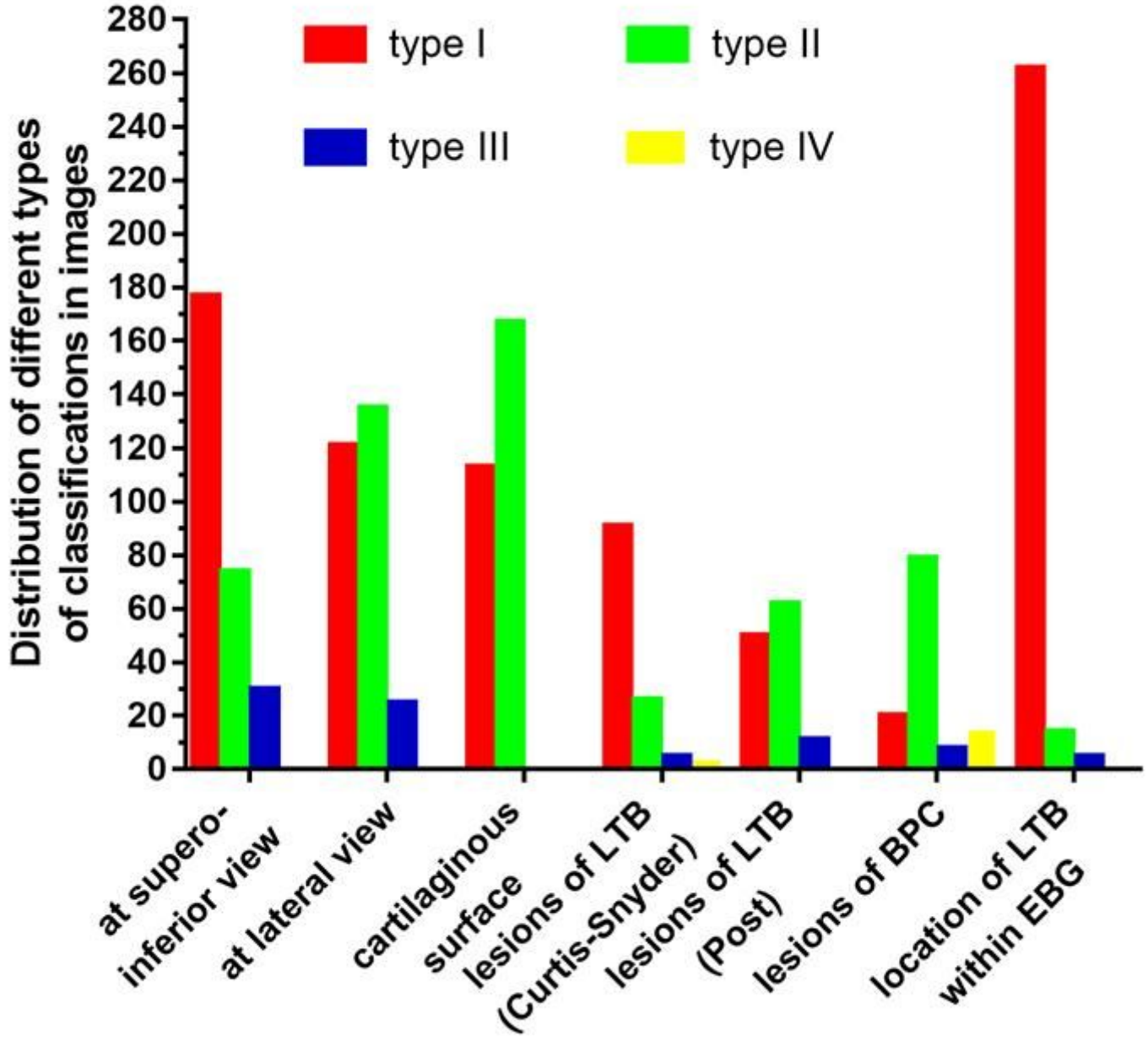

Figure 10

Distribution of different classification types on MRI.